

**Effects of titanium dioxide nanoparticles coupled with diode laser on optical properties of *in vitro* normal and cancerous human lung tissues studied with optical coherence tomography and diffuse reflectance spectra**

Lianpeng Zhou  
Guoyong Wu  
Huajiang Wei  
Zhouyi Guo  
Hongqin Yang  
Yonghong He  
Shusen Xie  
Ying Liu  
Qingan Meng

# Effects of titanium dioxide nanoparticles coupled with diode laser on optical properties of *in vitro* normal and cancerous human lung tissues studied with optical coherence tomography and diffuse reflectance spectra

Lianpeng Zhou,<sup>a</sup> Guoyong Wu,<sup>b</sup> Huajiang Wei,<sup>a,\*</sup> Zhouyi Guo,<sup>a</sup> Hongqin Yang,<sup>c</sup> Yonghong He,<sup>d</sup> Shusen Xie,<sup>c</sup> Ying Liu,<sup>a</sup> and Qingan Meng<sup>e</sup>

<sup>a</sup>South China Normal University, College of Biophotonics, MOE Key Laboratory of Laser Life Science & Institute of Laser Life Science, 55 Zhongshan Road, Guangzhou, Guangdong Province 510631, China

<sup>b</sup>Sun Yat-Sen University, the First Affiliated Hospital, Department of Surgery, 58 Zhongshan 2 Road, Guangzhou, Guangdong Province 510080, China

<sup>c</sup>Fujian Normal University, Key Laboratory of Optoelectronic Science and Technology for Medicine of Ministry of Education of China, 1 Keji Road, Fuzhou, Fujian 350007, China

<sup>d</sup>Tsinghua University, Graduate School at Shenzhen, 2279 Lishui Road, Shenzhen, Guangdong 518055, China

<sup>e</sup>Southwest Institute of Technical Physics, 7 People's South Road, Chengdu, Sichuan 610041, China

**Abstract.** The objective is to investigate the effects of two different sized (60 and 100 nm) titanium dioxide (TiO<sub>2</sub>) nanoparticles (NPs) penetration and accumulation in *in vitro* human normal lung (NL) tissue, lung squamous cell carcinoma (LSCC) tissue, and 650-nm diode laser-pretreated tissue on their optical properties studied with optical coherence tomography monitoring and diffuse reflectance (DR) spectra measurement. As with TiO<sub>2</sub> NPs penetrating into the tissues, the intensities of DR of the samples increase, and then the enhancements of DR and the attenuation coefficients of the tissues were quantitatively calculated. The results suggest that 650-nm diode laser pretreatment increased the amounts of TiO<sub>2</sub> NPs penetration and accumulation in NL and LSCC tissues, and the tissue optical properties were significantly influenced by accumulation of TiO<sub>2</sub> NPs. © 2015 Society of Photo-Optical Instrumentation Engineers (SPIE) [DOI: 10.1117/1.JBO.20.4.046003]

Keywords: titanium dioxide nanoparticle; accumulation; laser; optical coherence tomography; diffuse reflectance spectra.

Paper 140857R received Dec. 23, 2014; accepted for publication Mar. 16, 2015; published online Apr. 9, 2015.

## 1 Introduction

Lung cancer is the leading cause of cancer deaths in men and the second leading cause of cancer deaths in women, with approximately 1.6 million new cases of lung cancer diagnosed and 1.4 million deaths each year throughout the world.<sup>1-3</sup> Nonsmall cell lung cancer, which includes adenocarcinoma, squamous cell carcinoma, large cell carcinoma, and bronchioloalveolar carcinoma, accounts for nearly 85% of all cases of lung cancer.<sup>2,3</sup> Cigarette smoking is the most common etiological factor, accounting for about 80% of global lung cancer deaths in men and 50% of the deaths in women.<sup>4,5</sup> In addition, environmental exposures other than smoking may contribute to the incidence of lung cancer.<sup>6</sup>

With the development of nanotechnology, there has been a tremendous growth in the application of nanoparticles (NPs) for drug delivery systems, antibacterial materials, cosmetics, sunscreens, and electronics.<sup>7,8</sup> TiO<sub>2</sub> NPs, with the property of absorption and reflection of ultraviolet lights, are used extensively in a variety of cosmetics. TiO<sub>2</sub> fine particles, traditionally considered as poorly soluble, low toxicity particles, have been used as a “negative control” in many *in vitro* and *in vivo* particle toxicological studies.<sup>9</sup> However, this view was challenged after

Lee et al.<sup>10</sup> revealed that rats suffered from lung tumors after 2 years of exposure to high concentrations of fine TiO<sub>2</sub> particles. In recent years, TiO<sub>2</sub> NPs have been widely used in industrial and consumer products due to their stronger catalytic activity when compared with TiO<sub>2</sub> fine particles, which are due to their smaller sizes and larger surface area per unit mass. Nevertheless, studies have revealed that TiO<sub>2</sub> NPs are more toxic than TiO<sub>2</sub> fine particles.<sup>9,11,12</sup> Oberdorster et al.<sup>13</sup> have reported that TiO<sub>2</sub> NPs caused a greater pulmonary inflammatory response than TiO<sub>2</sub> fine particles at the same mass burden, with greater amounts of TiO<sub>2</sub> NPs entering the alveolar interstitium in the lungs. Li et al.<sup>14</sup> have shown that instilled TiO<sub>2</sub> NPs could induce lung damage and change the permeability of the alveolar-capillary barrier. Wide application of TiO<sub>2</sub> NPs confers substantial potential for human exposure and environmental release, which inevitably allows for a potential health risk to humans, livestock, and the ecosystem, especially the possible induction of lung cancer.<sup>13-15</sup> The potential adverse effects of TiO<sub>2</sub> NPs on lung tissue and their challenge to human health have raised particular concerns, therefore, it is very necessary to study the effects of TiO<sub>2</sub> NPs penetrating and accumulating in the human body, especially in human lung tissue.

\*Address all correspondence to: Huajiang Wei, E-mail: [weihj@sclu.edu.cn](mailto:weihj@sclu.edu.cn)

Although there have been numerous studies of TiO<sub>2</sub> NPs in biomedicine, most of them have focused on the study of toxicological information of TiO<sub>2</sub> NPs within different organs<sup>16,17</sup> while some studies focused on the research of TiO<sub>2</sub> NPs accumulation in human or animal skin.<sup>18,19</sup> Our group has reported the effects of NPs accumulation in *ex vivo* human colon tissue on tissue optical properties.<sup>20</sup> However, there are few studies that investigate the effects of TiO<sub>2</sub> NPs penetrating and accumulating in human normal lung (NL) and lung squamous cell carcinoma (LSCC) tissue on tissue optical properties. Herein, the issues are addressed using the methods of optical coherence tomography (OCT) imaging and diffuse reflectance (DR) spectra. OCT is a noninvasive technique for imaging biotissues at a depth of up to 2 mm with axial spatial resolution down to units of micrometers based on low-coherent interferometry in the near-infrared range of wavelengths (0.75 to 1.3 μm). In recent years, OCT has proved to be an efficient tool for the imaging of the superficial tissues of skin and mucous membranes.<sup>21,22</sup> DR spectra measurement is also a noninvasive method widely used in monitoring analyses concentrations in bulk tissue and investigating tissue optical parameters.<sup>23–27</sup> It is one of the simplest and most cost effective methods for understanding biological tissue characteristics. This technique involves detection and analysis of a portion of the incident light that undergoes multiple elastic scattering caused by inhomogeneities in the refractive index of the tissue.

With the development of medical laser techniques, lasers have been shown to have great advantages in enhancing transdermal drug delivery of not only small molecules but also of large and hydrophilic molecules. Lasers are different from ultrasound and are an established technology for drug delivery.<sup>28</sup> The displacement caused by ultrasound oscillates equally between positive and negative pressures, whereas the laser is a unipolar compression wave (positive pressure).<sup>29</sup> Reduction of light scattering has the potential to improve many current and novel diagnostic and therapeutic applications of lasers in medicine. A plethora of current and novel diagnostically and therapeutically useful applications of lasers in medicine will benefit from precise control over tissue optical properties and our ability to temporarily influence them. Studies have reported that after QS-Nd:YAG laser irradiation, both the concentration and penetration depth of methylene blue into biofilms were enhanced,<sup>30</sup> and the penetration of 5-fluorouracil into irradiated rabbit ear skin was increased.<sup>31</sup> In addition, Genina et al.<sup>18</sup> have reported that fractional laser microablation with Er:YAG laser allowed for efficient administering of NPs into the skin. Stump et al.<sup>32</sup>

have revealed that using an inexpensive 980 nm diode laser can significantly enhance the delivery of topically applied glycerol for optical skin clearing. However, there are few studies to investigate laser irradiation for improving NPs penetration into biological tissues. As a result, we try to use 650-nm diode laser irradiation to enhance TiO<sub>2</sub> NPs penetration into lung tissue and then investigate the induced changes of tissue optical properties.

In this study, in order to assess the effects of TiO<sub>2</sub> NPs on optical properties of human lung tissue for further understanding the interactions between TiO<sub>2</sub> NPs and lung tissue, we monitored the continuous process of two different sized TiO<sub>2</sub> NPs penetrating and accumulating in normal and cancerous lung tissues with OCT and DR spectra. In addition, 650-nm diode lasers were used to irradiate the lung tissues to enhance the amounts of TiO<sub>2</sub> NPs penetrating in the tissues and then evaluate the induced changes of tissue optical properties.

## 2 Materials and Methods

### 2.1 TiO<sub>2</sub> Nanoparticles Preparation and Transmission Electron Microscopy Measurements

In this study, 60 and 100 nm commercially available high purity (99.8%) rutile TiO<sub>2</sub> NPs (Aladdin Chemistry Co. Ltd, Shanghai, China) were used, which are the primary particle sizes of food grade TiO<sub>2</sub> and are also the main TiO<sub>2</sub> NPs sizes existing in personal care products.<sup>33</sup> A TiO<sub>2</sub> NPs suspension was prepared by dissolving TiO<sub>2</sub> powder in distilled water to a concentration of 1 mg/ml. TiO<sub>2</sub> NPs are highly aggregable; hence, the suspension was dispersed in an ultrasonic bath (the power of 35 W and the frequency of 43 to 45 kHz) for 30 to 40 min for thorough mixing of the content both in the process of preparation and immediately prior to use. High-resolution images of two different sized TiO<sub>2</sub> NPs were obtained via transmission electron microscopy (TEM). Samples were dropped to 400-mesh carbon-coated copper grids and dried for measurement. Without further preparation, the samples were evaluated in TEM (JEM-2100HR, JEOL, Japan). The TEM images are shown in Fig. 1.

### 2.2 Tissue Preparation and Laser Irradiation

Excised surgical human LSCC tissues were obtained from the First Affiliated Hospital of Sun Yat-Sen University, in which the study protocol was approved by the Ethics Committee and signed informed consents were obtained from all eight patients.

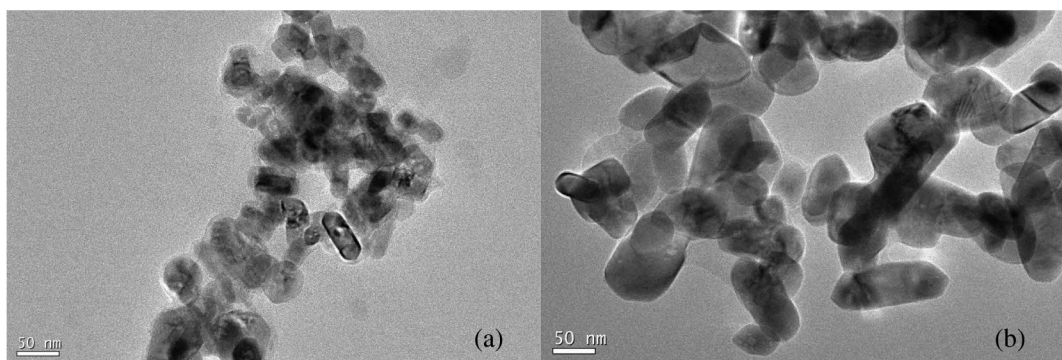


**Fig. 1** Transmission electron microscopy (TEM) images of TiO<sub>2</sub> NPs with two different sizes: (a) 60-nm TiO<sub>2</sub> NPs; and (b) 100-nm TiO<sub>2</sub> NPs.

All the lung tissues were stored in a refrigerator at  $-70^{\circ}\text{C}$  until measurement. NL tissues were peeled off from the edges of tumor tissues. The sample obtained from each patient was cut into 20 pieces in a freezing state, with lateral dimension of approximately  $1.2 \times 1.2 \text{ cm}^2$  and 5-mm thick, half of which are NL tissues, while the others are LSCC tissues. Therefore, a total of 160 pieces of specimens were prepared from all eight patients. The experiments were totally divided into 10 groups, eight of which were experimental groups and are shown in Table 1. The other two groups are NL and LSCC control groups, respectively. Each group contains 16 pieces of specimens from eight patients, half of which were used for OCT monitoring, and the other half were used for DR measurement, which means each measurement (OCT or DR spectra) was repeatedly tested eight times from eight different samples of eight patients.

At the beginning, samples were defrosted in physiological saline at room temperature for 30 min before application. In the laser irradiation experiments, all the samples used for OCT monitoring and DR measurement were irradiated by a 650-nm diode laser before any application. The diode laser (Nanjing Lichuang Laser Technology Co., Ltd., China) with an output power of 100 mW and a beam diameter of 5 mm was used and achieved a total fluence of about  $22.5 \text{ J/cm}^2$  with a duration of about 45 s on the tissue. As the length of OCT scanned area is 3 mm and the incident beam diameter of optical fiber spectrometer is about 4 mm, the area of diode laser irradiation on the tissue is enough for OCT and DR spectra measurements and the laser irradiation is almost uniform for the measurement area of OCT and DR spectra. The parameters were repeatedly tested, have been proven to be the optimal dose for enhancing penetration of  $\text{TiO}_2$  NPs by our unpublished data and cause no side effects. An infrared thermometer was used to dynamically monitor the temperature of the tissue surface during the laser irradiation.

### 2.3 Optical Coherence Tomography Monitoring

The experiments were implemented using a commercial spectral-domain OCT (SD-OCT) system (Shenzhen MOPTIM Imaging Technique Co., Ltd., China) working at a central wavelength of  $830 \pm 40 \text{ nm}$  with an optical power of 5 mW, a maximum image depth of 1.6 mm, a signal-to-noise ratio of 120 dB, and a length of the scanned area of 3 mm. The SD-OCT system, determined by the focal spot size of the probe beam, provides an axial resolution of  $12 \mu\text{m}$  and a transverse resolution of  $15 \mu\text{m}$  in free space. Two-dimensional (2-D) images are obtained by scanning the incident beam over the sample surface in the lateral direction and in-depth (A-scan) scanning by the interferometer. OCT images were acquired over a period of 240 min in 1-min intervals to record transient changes of optical tissue properties.

OCT images obtained in the experiment were stored in a computer for further postprocessing.

The selected region of each sample was monitored for about 8 to 10 min by the OCT system to get a baseline before any application. Then 25  $\mu\text{l}$  drops of  $\text{TiO}_2$  NPs suspension were applied on the lung tissue surface. The samples were irradiated by the laser before surface application of the NPs suspension. After the application of the NPs solution, the samples were immediately continuously monitored for the next 240 min at room temperature. Each sample was used only once.

### 2.4 Reflectance Measurements

The reflectance spectra of lung tissues were measured using a commercial optical fiber spectrometer (Ocean Optics, model: USB 4000) in the spectral range of 200 to 1100 nm. The tungsten halogen light source (Ocean Optics, model: LS-450) served as a source of light. The fiber-optic probe (Ocean Optics, model: USB 4000) consisting of seven fibers with an internal diameter  $400 \mu\text{m}$  and a numerical aperture 0.2 was used in the measurements. The central fiber served to collect the diffuse reflected radiation, while the surrounding six fibers were used for illumination of the sample. The probe was placed at a distance of 2 mm from the sample surface and registered the signal, which was averaged over the area of the radiation collection. The spectra were calibrated against a DR standard of  $\text{BaSO}_4$  with a smooth surface. All spectra measurements were recorded with the integration time set to 100 ms. The measurements were recorded and stored into a computer for further postprocessing.

DR spectra were acquired over a period of 240 min in 30-min intervals to record transient changes of optical tissue properties after surface application of the NPs suspension. The spectra obtained before any administration were used as a control. The suspension of the sample surface was wiped gently with a tampon wetted with saline prior to DR measurement. After each measurement, the  $\text{TiO}_2$  NPs suspension was applied again on the tissue. During the procedure, the samples were placed in a Petri dish with a small volume of saline to prevent the change in the optical properties due to dehydration. Each sample was used only once.

### 2.5 Data Processing

In order to characterize the changes in optical properties of lung tissues during the penetration and accumulation of  $\text{TiO}_2$  NPs, the attenuation coefficients of each sample were calculated from the 2-D OCT image. The total OCT attenuation coefficient of the tissue is the sum of the absorption coefficient  $\mu_a$  and scattering coefficient  $\mu_s$ :  $\mu_t = \mu_a + \mu_s$ , and can be determined from the slope of the A-scan of the OCT signal measured for the

**Table 1** Groups and treatment in the experiments.

Groups	Normal lung (NL) tissue	Groups	Lung squamous cell carcinoma (LSCC) tissue
A	60-nm $\text{TiO}_2$ NPs	E	60-nm $\text{TiO}_2$ NPs
B	60-nm $\text{TiO}_2$ NPs/laser	F	60-nm $\text{TiO}_2$ NPs/laser
C	100-nm $\text{TiO}_2$ NPs	G	100-nm $\text{TiO}_2$ NPs
D	100-nm $\text{TiO}_2$ NPs/laser	H	100-nm $\text{TiO}_2$ NPs/laser

region of interest.<sup>34–37</sup> In the superficial layers of many tissues, a single-scattering model can be adequately used.<sup>36,37</sup> In accordance with the single-scattering model, the measured signal in the OCT system is defined as<sup>34–37</sup>

$$[\langle i^2(z) \rangle]^{\frac{1}{2}} \approx (\langle i^2 \rangle_0)^{\frac{1}{2}} [\exp(-2\mu_t z)]^{\frac{1}{2}}, \quad (1)$$

where the  $\langle i^2(z) \rangle$  is the photodetector heterodyne signal current received by the OCT system from the probing depth  $z$  and  $\langle i^2 \rangle_0$  is the mean square heterodyne signal. In OCT, the intensity of the optical reflection,  $R(z) \propto [\langle i^2(z) \rangle]^{\frac{1}{2}}$ , via the tissue probing depth  $z$  is measured. The reflectance depends on the optical properties of tissue, i.e., the total attenuation coefficient  $\mu_t$ . Thus, in the single-scattering model, the reflected power can be approximately proportional to  $-\mu_t z$ , i.e.,<sup>34</sup>

$$R(z) = I_0 a(z) \times \exp(-\mu_t z), \quad (2)$$

where  $I_0$  is the incident light intensity launched into the tissue sample, and  $a(z)$  is the reflectivity of the tissue at depth  $z$ .  $a(z)$  is linked to the local refractive index and backscattering property of the tissue.<sup>34</sup> However, the reflectivity  $a(z)$  is considered as weakly dependent on depth for a homogeneous tissue layer. Therefore,  $\mu_t$  can be obtained theoretically from the reflectance measurements at two different depths,  $z_1$  and  $z_2$ .<sup>34–37</sup>

$$\mu_t = \frac{1}{\Delta z} \ln \left[ \frac{R(z_1)}{R(z_2)} \right], \quad (3)$$

where  $\Delta z = |z_1 - z_2|$ . As noise is inevitable in the measurement, a final result should be obtained by the use of a best-fit exponential curve technique in order to improve the accuracy of the determined value of  $\mu_t$ . An averaged optical intensity profile that represents the reflected light intensity distribution in depth is obtained by averaging the 2-D image laterally over 1 mm, which is wide enough for speckle noise suppression.

Figure 2 shows the example for calculating the attenuation coefficients of lung tissues. For calculation, we selected the region [white rectangle in Fig. 2(a)] from which OCT depth intensity profiles with a corresponding exponential best-fit curve were obtained. The region of interest [red rectangle in Fig. 2(a)] was selected from a depth of 130  $\mu\text{m}$  to a depth of 287  $\mu\text{m}$ , where the OCT signal distribution is relatively smooth. The fitted curve [red curve in Fig. 2(b)] in the region of interest allows evaluating the attenuation coefficient.

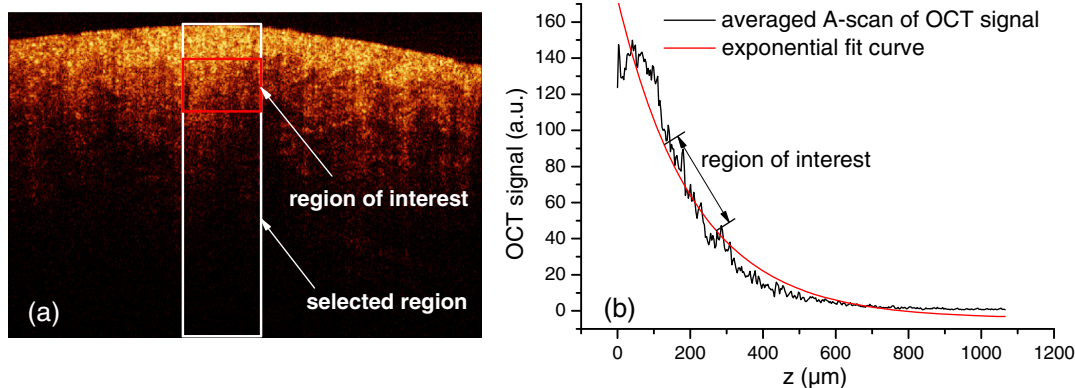


**Fig. 2** Typical B-scan of lung tissue with (a) marked selection region and region of interest and (b) plot of the averaged A-scan and the exponential best-fit curve for calculating attenuation coefficient.

In the spectroscopic measurements, the changes of reflectance induced by the NPs solution were quantitatively evaluated by calculating the increase in DR after 60-, 120-, 180-, and 210-min treatment. The increase in DR by the solutions at the time intervals of treatment was calculated as Eq. (4).<sup>38,39</sup>

$$\Delta R = \frac{R_{x \min} - R_{\text{control}}}{R_{\text{control}}} \times 100\%, \quad (4)$$

where  $R_{\text{control}}$  and  $R_{x \min}$  are the measured diffuse reflectances at 543 and 578 nm of each group of samples before and after  $x$  min treatment in different ways. The reason for selecting 543 and 578 nm to assess reflectance is that these wavelengths represent visible wavelength with skin oxyhemoglobin absorption.<sup>40–42</sup>

## 2.6 Statistical Analysis

The data from all samples were presented as means  $\pm$  SD and analyzed by an statistical product and service solutions 20.0 software paired-test. For each measurement (OCT or DR spectra) of every group, eight samples from eight patients were repeatedly tested and the data obtained from the measurement were used for statistics. The  $p < 0.05$  value indicated significant difference.

## 3 Results and Discussion

Figures 3(a)–3(d) illustrate the dynamic changes of DR as a function of time elapsed after the NL tissue samples were topically treated with 60-nm TiO<sub>2</sub> NPs alone, 60-nm TiO<sub>2</sub> NPs in combination with laser, 100-nm TiO<sub>2</sub> NPs alone, and 100-nm TiO<sub>2</sub> NPs in combination with laser, respectively. The lowest black lines in Figs. 3(a) and 3(c) represent spectra that were measured from the intact lung tissues without any treatment, whereas the lines in Figs. 3(b) and 3(d) represent spectra that were measured immediately from laser-treated tissues. There is a distinguishable difference between the spectra with and without laser irradiation. With the laser irradiation, the DR spectra of laser-treated tissues were relatively lower than the spectra of intact tissues. The increase in the intensity of radiation reflected from the sample was observed, which is related to a substantial increase of the scattering coefficient of the tissue, promoted by the NPs located in the lung tissues. In the spectroscopic measurements, the absorption bands of blood hemoglobin at the wavelengths 416 (Soret band), 543, and 578 nm are very pronounced. Figure 4 shows the enhancement of DR for

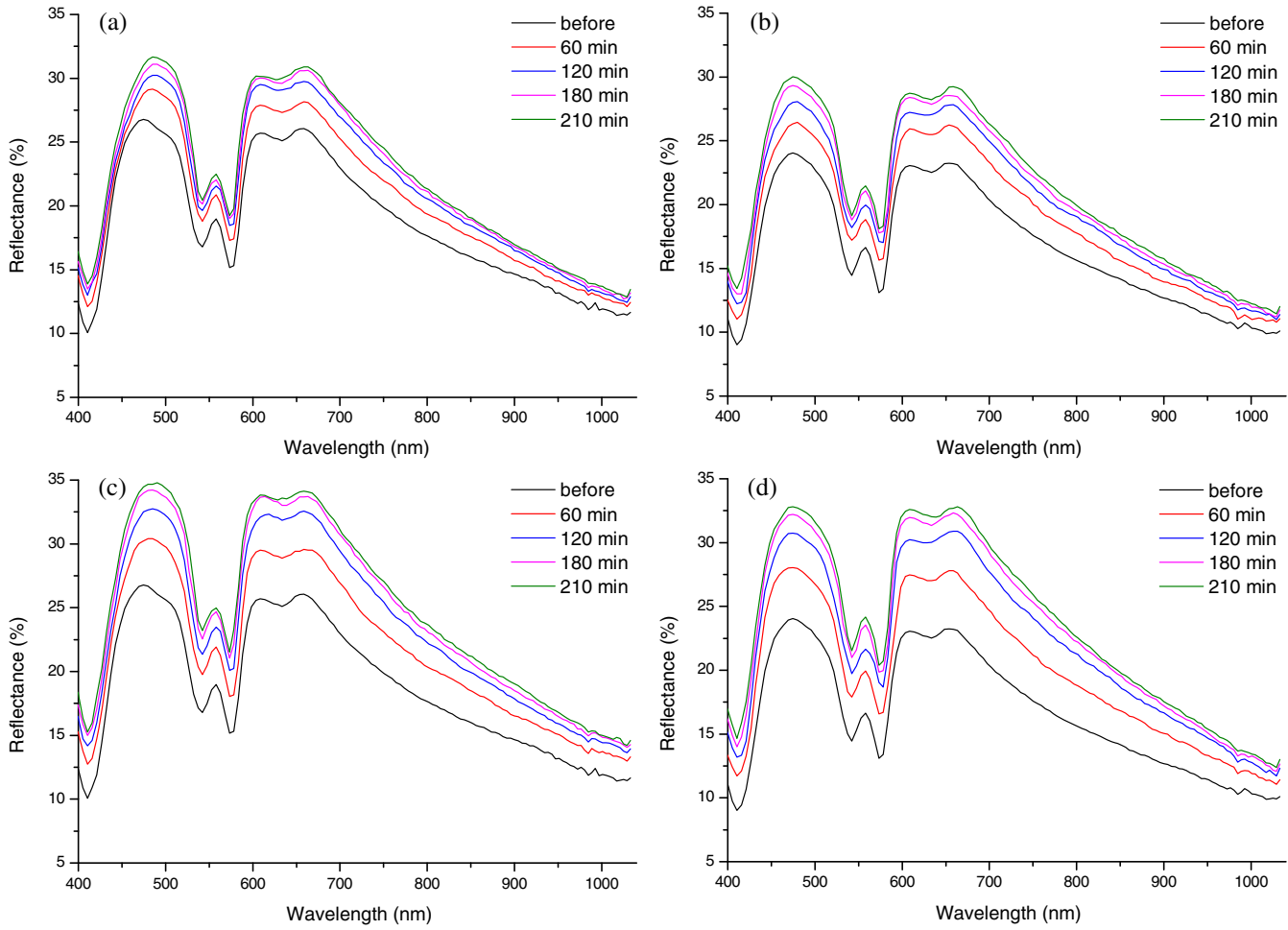


**Fig. 3** Measured diffuse reflectance spectra over 400 to 1100 nm for *in vitro* human normal lung (NL) tissue before and after different applications at 60, 120, 180, and 210 min: (a) NL samples with 60-nm TiO<sub>2</sub>; (b) NL samples with 60-nm TiO<sub>2</sub>/laser; (c) NL samples with 100-nm TiO<sub>2</sub>; and (d) NL samples with 100-nm TiO<sub>2</sub>/laser.

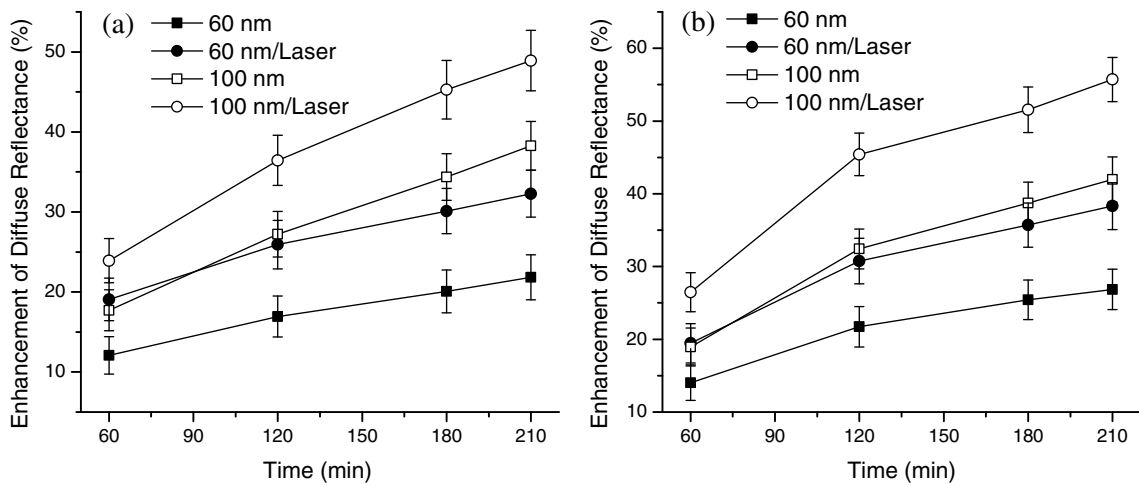


**Fig. 4** Enhancement of diffuse reflectance at wavelengths (a) 543 nm and (b) 578 nm for human NL tissue after different applications of TiO<sub>2</sub> NPs solution on the tissues at 60, 120, 180, and 210 min, respectively.

NL tissues at the wavelengths 543 and 578 nm per time of penetration of 60- and 100-nm TiO<sub>2</sub> NPs with and without laser irradiation. As with TiO<sub>2</sub> NPs penetration into the tissues, the DR of the samples increases; however, after the tissues are irradiated by laser, the enhancement of DR is markedly larger than the tissues treated with the same type of NPs alone at the same time. Additionally, the enhancement of DR is higher for 100-nm TiO<sub>2</sub> NPs than for 60-nm TiO<sub>2</sub> NPs under the same conditions. This may be caused by the fact that 100-nm TiO<sub>2</sub> NPs have a larger backscattering compared with 60-nm TiO<sub>2</sub> NPs. Figs. 5(a)–5(d) illustrate the dynamic changes of DR per time of LSCC tissues treated with 60-nm TiO<sub>2</sub> NPs alone, 60-nm TiO<sub>2</sub> NPs in combination with laser, 100-nm TiO<sub>2</sub> NPs alone, and 100-nm TiO<sub>2</sub> NPs in combination with laser, respectively. By comparing Figs. 3 and 5, it is obvious that the spectra of LSCC tissues are very different from the spectra of NL tissues in the amplitudes. The amplitudes for the spectra of NL tissue are obviously higher as compared with the spectra of LSCC tissue under the same conditions. The wavelengths of the main peaks of both NL and LSCC tissues and the absorption bands of blood hemoglobin at the wavelengths 416, 543, and 578 nm are not changed.<sup>42,43</sup> Figure 6 shows the enhancement of DR for LSCC tissue at the wavelengths 543 and 578 nm per time of penetration of

the 60- and 100-nm TiO<sub>2</sub> NPs with and without laser irradiation. The results show that the enhancement of DR for LSCC tissue with laser irradiation is significantly larger than for the tissue without laser irradiation when treated with the same type of NPs, and the enhancement of DR is bigger for 100-nm TiO<sub>2</sub> NPs than for 60-nm TiO<sub>2</sub> NPs under the same conditions. The results are similar to the previous results for NL tissues. Moreover, the enhancement of DR for LSCC tissue is markedly larger than that for NL tissue when under the same treatment. The difference in optical properties between NL and LSCC tissue may be induced by the morphological and structural differences between the two types of tissues, such as larger nuclei, the higher nuclear-to-cytoplasmic ratio in tumor cells, and the higher regional tumor cell density of the tumor tissues.<sup>43</sup> As the result, LSCC tissue may be easier to penetrate compared with NL tissue, thus, more NPs would spread into the LSCC tissue and induce a higher enhancement of DR.

The attenuation coefficients of each group at different times were calculated from the data of the best exponential fit curve corresponding to the averaged intensity profiles. All the attenuation coefficients of NL and LSCC tissues are shown in Table 2. Figs. 7 and 8 present the changes in the attenuation coefficients of NL and LSCC treated with 60-nm TiO<sub>2</sub> NPs, 60-nm TiO<sub>2</sub> NPs/laser, 100-nm TiO<sub>2</sub> NPs, and 100-nm TiO<sub>2</sub> NPs/laser,

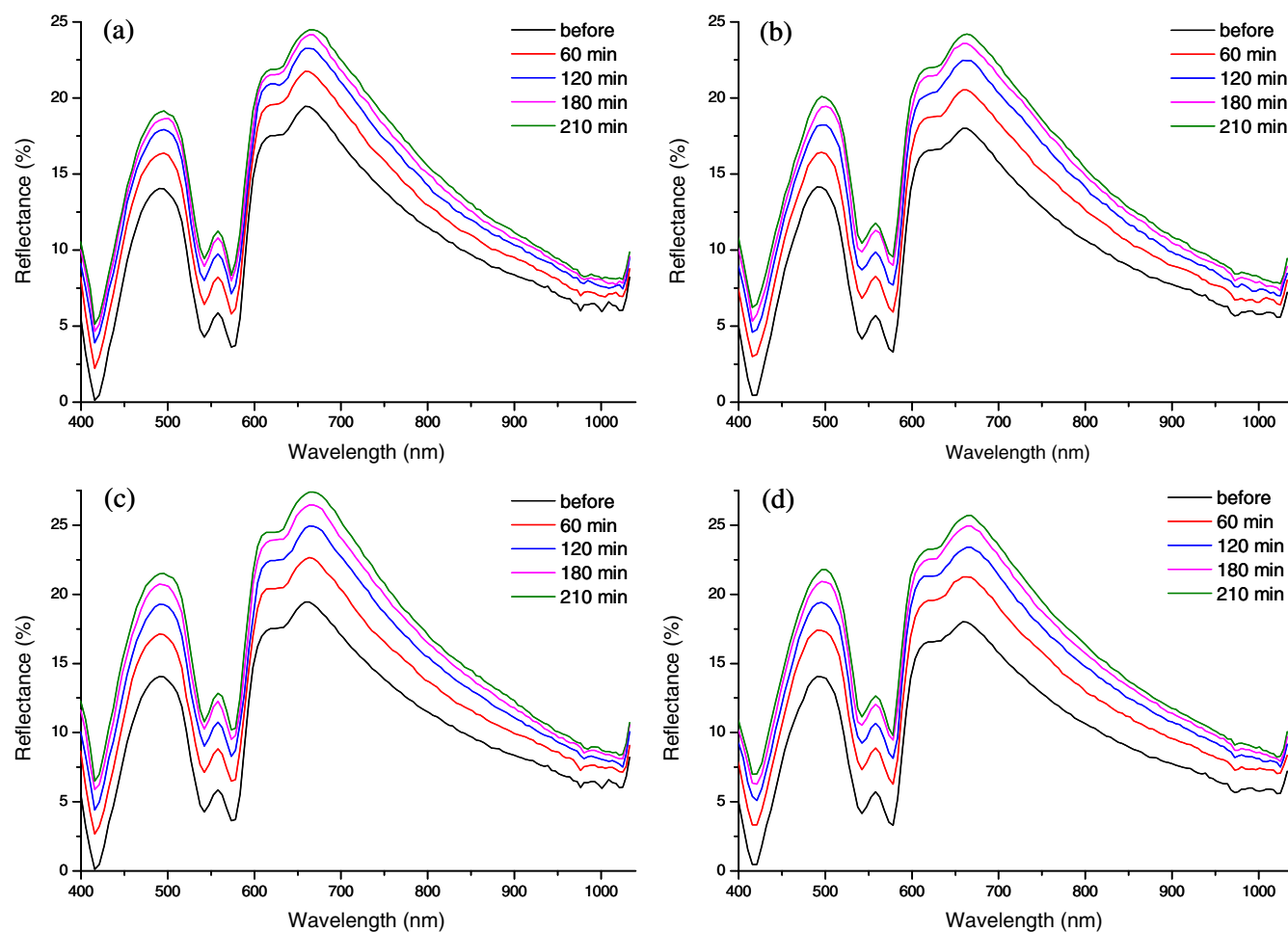


**Fig. 5** Measured diffuse reflectance spectra over 400 to 1100 nm for *in vitro* human lung squamous cell carcinoma (LSCC) tissue before and after different applications at 60, 120, 180, and 210 min: (a) LSCC samples with 60-nm TiO<sub>2</sub>; (b) LSCC samples with 60-nm TiO<sub>2</sub>/laser; (c) LSCC samples with 100-nm TiO<sub>2</sub>; and (d) LSCC samples with 100-nm TiO<sub>2</sub>/laser.

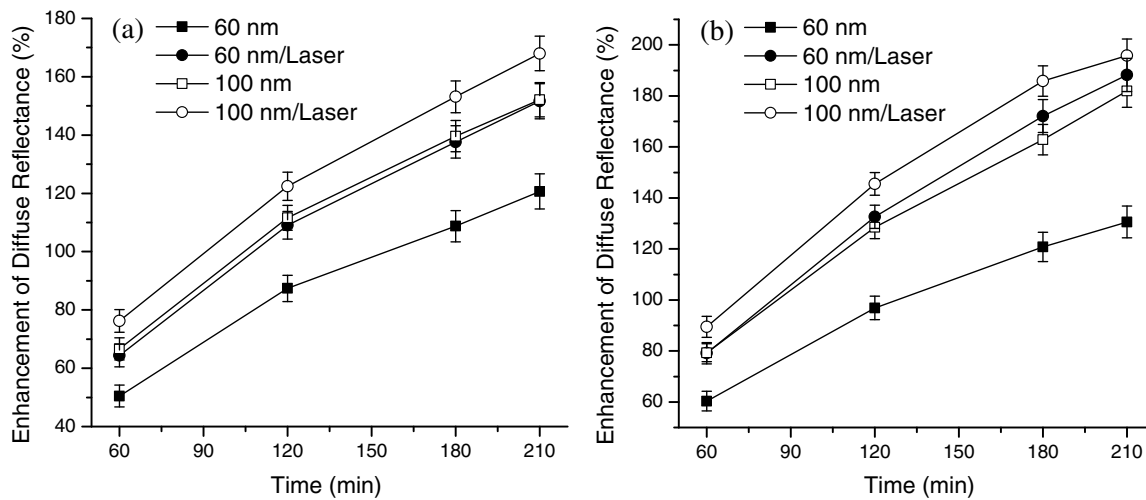


**Fig. 6** Enhancement of diffuse reflectance at wavelengths (a) 543 nm and (b) 578 nm for human LSCC tissue after different applications of TiO<sub>2</sub> NPs solution on the tissues at 60, 120, 180, and 210 min, respectively.

respectively. In Figs. 7(a)–7(d), the attenuation coefficients of NL tissue are about  $4.66 \pm 0.21 \text{ mm}^{-1}$  for 60-nm TiO<sub>2</sub> NPs treatment and  $4.83 \pm 0.24 \text{ mm}^{-1}$  for 100-nm TiO<sub>2</sub> NPs treatment, then they changed to be  $3.29 \pm 0.12 \text{ mm}^{-1}$  for 60-nm TiO<sub>2</sub> NPs treatment at about 163 min and  $3.42 \pm 0.13 \text{ mm}^{-1}$  for 100-nm TiO<sub>2</sub> NPs treatment at about 175 min when the penetration process reached the stable state. As with laser pretreatment, the starting values of the attenuation coefficients of NL tissue are  $4.46 \pm 0.11 \text{ mm}^{-1}$  for 60-nm TiO<sub>2</sub> NPs treatment and  $4.73 \pm 0.11 \text{ mm}^{-1}$  for 100-nm TiO<sub>2</sub> NPs treatment, then it took about 151 min for the 60-nm TiO<sub>2</sub> NPs treatment and 156 min for the 100-nm TiO<sub>2</sub> NPs treatment to reach the stable state, and the values changed to  $2.28 \pm 0.08$  and  $2.67 \pm 0.07 \text{ mm}^{-1}$ , respectively. Similarly, as to LSCC tissue (Fig. 8), the attenuation coefficients were calculated to be  $10.87 \pm 0.58$ ,  $10.28 \pm 0.43$ ,  $11.85 \pm 0.61$ , and  $11.48 \pm 0.59 \text{ mm}^{-1}$  at 0 min for treatment of 60-nm TiO<sub>2</sub> NPs, 60-nm TiO<sub>2</sub> NPs/laser, 100-nm TiO<sub>2</sub> NPs, and 100-nm TiO<sub>2</sub> NPs/laser, respectively. Then, as with NPs penetrating into LSCC tissues, the penetration of TiO<sub>2</sub> NPs at LSCC tissues took approximately 124, 108, 132, and 115 min for the treatment of 60-nm TiO<sub>2</sub> NPs, 60-nm TiO<sub>2</sub> NPs/laser, 100-nm TiO<sub>2</sub> NPs, and 100-nm TiO<sub>2</sub> NPs/laser, respectively, to reach the stable state. Their attenuation coefficients changed to  $5.38 \pm 0.31$ ,  $4.55 \pm 0.27$ ,  $5.56 \pm 0.24$ , and  $5.42 \pm 0.33 \text{ mm}^{-1}$ , respectively.

As is seen from the results of all the data in Figs. 7 and 8, using a laser pretreatment, for both of NL and LSCC tissues the penetration of TiO<sub>2</sub> NPs into the tissues was dramatically increased and accelerated as compared with the same kind of NPs treatment alone. Moreover, with the same treatment, the penetration of TiO<sub>2</sub> NPs in LSCC tissue is much faster than that in NL tissue; whereas for the same type of tissue, the penetration of 100-nm TiO<sub>2</sub> NPs in the tissue is slightly slower than 60-nm TiO<sub>2</sub> NPs. This is very consistent with the former results of DR spectra. The morphological and structural differences of lung tissues significantly affect the penetration of TiO<sub>2</sub> NPs. Different lung pathologies can affect the extracellular matrix.<sup>44</sup> Lung’s physiological behavior reflects both the mechanical properties of the individual tissue components and their complex structural organization and thus induces the differences of permeability of lung tissue. This is well illustrated in our previous study, in which Wei et al.<sup>45</sup> assessed the effects of ultrasound-mediated glucose on the permeability of normal, benign, and cancerous human lung tissues with OCT. During the laser irradiation, the temperature rise of the tissue surfaces was almost up to 8°C. Some studies have revealed that the transient photothermal effect could disrupt the stratum corneum and enhance transdermal drug delivery.<sup>30,31,46,47</sup> However, few studies revealed the physical and physiological mechanisms of diode laser irradiation for improving NPs penetration into lung tissues.

**Table 2** The attenuation coefficients of NL and LSCC tissues and the time required to reach the stable state.

Treatment	NL/LSCC tissue		
	Initial value (mm <sup>-1</sup> )	Stable value (mm <sup>-1</sup> )	Stable time (min)
60-nm TiO <sub>2</sub> NPs	4.66 ± 0.21/10.87 ± 0.58	3.29 ± 0.12/5.38 ± 0.31	163/124
60-nm TiO <sub>2</sub> NPs/laser	4.46 ± 0.11/10.28 ± 0.43	2.28 ± 0.08/4.55 ± 0.27	151/108
100-nm TiO <sub>2</sub> NPs	4.83 ± 0.24/11.85 ± 0.61	3.42 ± 0.13/5.56 ± 0.24	175/132
100-nm TiO <sub>2</sub> NPs/laser	4.73 ± 0.11/11.48 ± 0.59	2.67 ± 0.07/5.42 ± 0.33	156/115

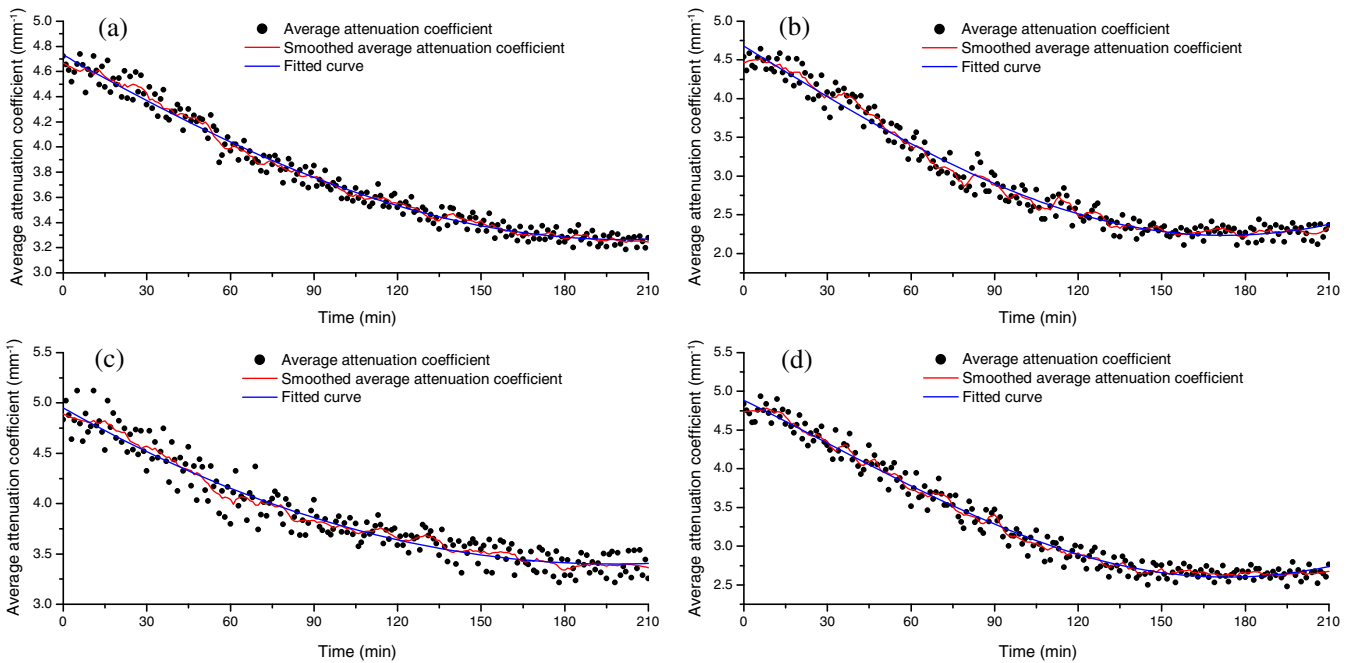


**Fig. 7** Average attenuation coefficients of NL tissue after different applications of two-sized TiO<sub>2</sub> NPs solution: (a) NL samples with 60-nm TiO<sub>2</sub>; (b) NL samples with 60-nm TiO<sub>2</sub>/laser; (c) NL samples with 100-nm TiO<sub>2</sub>; and (d) NL samples with 100-nm TiO<sub>2</sub>/laser.

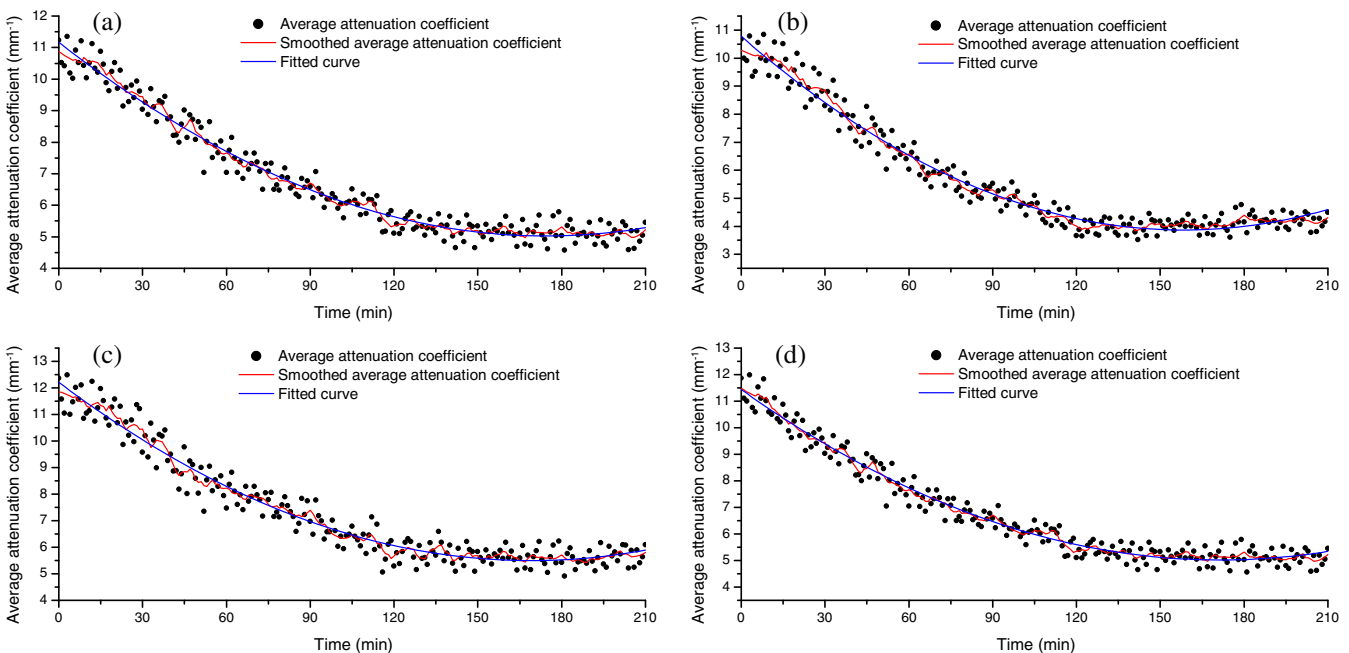


**Fig. 8** Average attenuation coefficients of LSCC tissue after different applications of two-sized TiO<sub>2</sub> NPs solution: (a) LSCC samples with 60-nm TiO<sub>2</sub>; (b) LSCC samples with 60-nm TiO<sub>2</sub>/laser; (c) LSCC samples with 100-nm TiO<sub>2</sub>; and (d) LSCC samples with 100-nm TiO<sub>2</sub>/laser.

As for this study, the temperature rise of the sample caused by laser irradiation may be the main cause of the increase in TiO<sub>2</sub> NPs penetration. But it is still worth further investigation into the mechanisms of diode laser irradiation for improving NPs penetration into lung tissues.

#### 4 Conclusions

This study considered the effects of two-sized TiO<sub>2</sub> NPs on the optical properties of human lung tissues, including NL and

LSCC tissues. Our results show the penetration process of TiO<sub>2</sub> NPs with both sizes (60 and 100 nm) in LSCC tissue is faster than that in NL tissue and that 60-nm TiO<sub>2</sub> NPs penetrate and accumulate faster than 100-nm TiO<sub>2</sub> NPs in the same type of lung tissue. In addition, the use of an inexpensive diode laser can significantly enhance the penetration of topically applied TiO<sub>2</sub> NPs in the tissue. Moreover, results of our studies show that OCT and DR provide an ideal tool to perform qualitative and quantitative analyses of the TiO<sub>2</sub> NPs penetration and

accumulation in lung tissue to reveal the localization of NPs within the tissues and to investigate the changes in optical properties of biotissue induced by NPs. However, the findings in this study and the effects of laser irradiation should be further tested in the future.

### Acknowledgments

This work was supported by the National Natural Science Foundation of China (Grant Nos. 60778047, 61335011, 61275187, and 81071790), Specialized Research Fund for the Doctoral Program of Higher Education of China (Grant Nos. 20114407110001 and 200805740003), the Science and Technology Innovation Project of the Education Department of Guangdong Province of China, the Natural Science Foundation of Guangdong Province of China (Grant Nos. 06025080 and 9251063101000009), Technique invention program of Guangdong Province (2013KJCX0052), the Science and Technology Project of Guangdong Province (2012A080203008), and Key Laboratory of Optoelectronic Science and Technology for Medicine (Fujian Normal University), Ministry of Education, China (Grant No. JYG1202).

### References

1. A. Jemal et al., "Global patterns of cancer incidence and mortality rates and trends," *Cancer Epidemiol., Biomarkers Prev.* **19**(8), 1893–1907 (2010).
2. S. S. Ramalingam, T. K. Owonikoko, and F. R. Khuri, "Lung cancer: new biological insights and recent therapeutic advances," *Ca-Cancer J. Clin.* **61**(2), 91–112 (2011).
3. A. Hurria and M. G. Kris, "Management of lung cancer in older adults," *Ca-Cancer J. Clin.* **53**(6), 325–341 (2003).
4. M. Ezzati et al., "Role of smoking in global and regional cancer epidemiology: current patterns and data needs," *Int. J. Cancer* **116**, 963–971 (2005).
5. M. Ezzati and A. D. Lopez, "Estimates of global mortality attributable to smoking in 2000," *Lancet* **362**, 847–852 (2003).
6. P. Boffetta and F. Nyberg, "Contribution of environmental factors to cancer risk," *Br. Med. Bull.* **68**, 71–94 (2003).
7. E. R. Kisin et al., "Single-walled carbon nanotubes: geno- and cytotoxic effects in lung fibroblast V79 cells," *J. Toxicol. Environ. Health, Part A* **70**, 2071–2079 (2007).
8. T. A. Robertson, W. Y. Sanchez, and M. S. Roberts, "Are commercially available nanoparticles safe when applied to the skin," *J. Biomed. Nanotechnol.* **6**, 452–468 (2010).
9. J. Zhao et al., "Titanium dioxide (TiO<sub>2</sub>) nanoparticles induce JB6 cell apoptosis through activation of the caspase-8/Bid and mitochondrial pathways," *J. Toxicol. Environ. Health, Part A* **72**, 1141–1149 (2009).
10. K. P. Lee, H. J. Trochimowicz, and C. F. Reinhardt, "Pulmonary response of rats exposed to titanium dioxide (TiO<sub>2</sub>) by inhalation for two years," *Toxicol. Appl. Pharmacol.* **79**, 179–192 (1985).
11. E. Fabian et al., "Tissue distribution and toxicity of intravenously administered titanium dioxide nanoparticles in rats," *Arch. Toxicol.* **82**, 151–157 (2008).
12. G. Oberdörster, "Pulmonary effects of inhaled ultrafine particles," *Int. Arch. Occup. Environ. Health* **74**(1), 1–8 (2000).
13. G. Oberdörster, J. Ferin, and B. E. Lehnert, "Correlation between particle size, *in vivo* particle persistence, and lung injury," *Environ. Health Perspect.* **102**, 173–179 (1994).
14. Y. Li et al., "Systematic influence induced by 3 nm titanium dioxide following intratracheal instillation of mice," *J. Nanosci. Nanotechnol.* **10**, 8544–8549 (2010).
15. T. C. Long et al., "Nanosize titanium dioxide stimulates reactive oxygen species in brain microglia and damages neurons *in vitro*," *Environ. Health Perspect.* **115**, 1631–1637 (2007).
16. G. Liang et al., "Influence of different sizes of titanium dioxide nanoparticles on hepatic and renal functions in rats with correlation to oxidative stress," *J. Toxicol. Environ. Health, Part A* **72**, 740–745 (2009).
17. J. Li et al., "Comparative study on the acute pulmonary toxicity induced by 3 and 20 nm TiO<sub>2</sub> primary particles in mice," *Environ. Toxicol. Pharmacol.* **24**, 239–244 (2007).
18. E. A. Genina et al., "Transcutaneous delivery of micro- and nanoparticles with laser microporation," *J. Biomed. Opt.* **18**(11), 111406 (2013).
19. M. A. Sirotkina et al., "Continuous optical coherence tomography monitoring of nanoparticles accumulation in biological tissues," *J. Nanopart. Res.* **13**, 283–291 (2011).
20. Y. Q. Zhang et al., "Effect of differently sized nanoparticles accumulation on the optical properties of *in vitro* normal and adenomatous human colon tissue with OCT imaging and diffuse reflectance spectra," *Laser Phys. Lett.* **11**, 085901 (2014).
21. F. I. Feldchtein et al., "Coherence domain optical methods in biomedical science, and clinical application," *Proc. SPIE* **4956**, 89–94 (2003).
22. E. V. Zagaynova et al., "*In vivo* study of contrasting properties of gold nanoshells for optical coherence tomography," *Proc. SPIE* **6633**, 663316 (2007).
23. N. Shah et al., "Noninvasive functional optical spectra of human breast tissue," *Proc. Natl. Acad. Sci. U. S. A.* **98**, 4420–4425 (2001).
24. G. Zonios et al., "Diffuse reflectance spectra of human adenomatous colon polyps *in vivo*," *Appl. Opt.* **38**, 6628–6637 (1999).
25. E. L. Hull and T. H. Foster, "Steady-state reflectance spectra in the P3 approximation," *J. Opt. Soc. Am. A* **18**, 584–599 (2001).
26. R. T. Zaman et al., "*In vivo* detection of gold nanoshells in tumors using diffuse optical spectroscopy," *IEEE J. Sel. Top. Quant.* **13**(6), 1715–1720 (2007).
27. D. Fixler and R. Ankri, "Subcutaneous gold nanorods detection with diffusion reflection measurement," *J. Biomed. Opt.* **18**, 061226 (2013).
28. S. Mitragotri and J. Kost, "Low-frequency sonophoresis: a review," *Adv. Drug Delivery Rev.* **56**, 589–601 (2004).
29. A. G. Doukas and T. J. Flotte, "Physical characteristics and biological effects of laser-induced stress waves," *Ultrasound Med. Biol.* **22**, 151–164 (1996).
30. M. Ogura et al., "Photomechanical wave-assisted drug delivery in oral multispecies biofilms," *World J. Microbiol. Biotechnol.* **23**(11), 1637–1646 (2007).
31. C. Gómezv et al., "Laser treatments on skin enhancing and controlling transdermal delivery of 5-fluorouracil," *Lasers Surg. Med.* **40**(1), 6–12 (2008).
32. O. F. Stumpp et al., "Enhancement of transepidermal skin clearing agent delivery using a 980 nm diode laser," *Lasers Surg. Med.* **37**, 278–285 (2005).
33. A. Weir et al., "Titanium dioxide nanoparticles in food and personal care products," *Environ. Sci. Technol.* **46**, 2242–2250 (2012).
34. R. K. Wang and V. V. Tuchin, "Optical coherence tomography: light scattering and imaging enhancement," Chapter 16 in *Handbook of Coherent-Domain Optical Methods*, V. V. Tuchin, Ed., pp. 665–742, Springer, New York (2013).
35. D. Levitz et al., "Determination of optical scattering properties of highly-scattering media in optical coherence tomography images," *Opt. Express* **12**(2), 249–259 (2004).
36. Y. Yang et al., "Optical scattering coefficient estimated by optical coherence tomography correlates with collagen content in ovarian tissue," *J. Biomed. Opt.* **16**, 090504 (2011).
37. L. Thrane, H. T. Yura, and P. E. Andersen, "Analysis of optical coherence tomography systems based on the extended Huygens-Fresnel principle," *J. Opt. Soc. Am. A* **17**, 484–490 (2000).
38. X. Q. Xu and R. K. Wang, "Synergistic effect of hyperosmotic agents of dimethyl sulfoxide and glycerol on optical clearing of gastric tissue studied with near infrared spectra," *Phys. Med. Biol.* **49**, 457–468 (2004).
39. J. Y. Jiang and R. K. Wang, "Comparing the synergistic effects of oleic acid and dimethyl sulfoxide as vehicles for optical clearing of skin tissue *in vitro*," *Phys. Med. Biol.* **49**, 5283–5294 (2004).
40. W. G. Zijlstra and A. Buursma, "Spectrophotometry of hemoglobin: absorption spectra of bovine oxyhemoglobin, deoxyhemoglobin, carboxyhemoglobin, and methemoglobin," *Comp. Biochem. Physiol.* **118**, 743–749 (1997).
41. E. Salomatina and A. N. Yaroslavsky, "Evaluation of the *in vivo* and *in vitro* optical properties in a mouse ear model," *Phys. Med. Biol.* **53**, 2797–2807 (2008).

42. A. N. Bashkatov et al., "Optical properties of human skin, subcutaneous and mucous tissues in the wavelength range from 400 to 2000 nm," *J. Phys. D: Appl. Phys.* **38**, 2543–2555 (2005).
43. M. G. Ghosn et al., "Permeability of hyperosmotic agent in normal and atherosclerotic vascular tissues," *J. Biomed. Opt.* **13**(1), 010505 (2008).
44. D. S. Faffe and W. A. Zin, "Lung parenchymal mechanics in health and disease," *Physiol. Rev.* **89**(3), 759–775 (2009).
45. H. J. Wei et al., "Assessment of the effects of ultrasound-mediated glucose on permeability of normal, benign, and cancerous human lung tissues with the Fourier-domain optical coherence tomography," *J. Biomed. Opt.* **17**, 116006 (2012).
46. O. Lademann et al., "Application of a plasma-jet for skin antiseptics: analysis of the thermal action of the plasma by laser scanning microscopy," *Laser Phys. Lett.* **7**(6), 458–462 (2010).
47. J. W. Lee et al., "Microsecond thermal ablation of skin for transdermal drug delivery," *J. Controlled Release* **154**(1), 58–68 (2011).

**Lianpeng Zhou** is a graduate student in the MOE Key Laboratory of Laser Life Science and Institute of Laser Life Science, College of Biophotonics at South China Normal University, China. His focus is histological diagnosis and control of optical properties of tissues using optical coherence tomography.

**Guoyong Wu** is a professor in the Department of Chest Surgery at the First Affiliated Hospital of Sun Yat-sen University, Guangzhou, China. He is mainly engaged in thoracic surgery and correlated research. His research interests include correction and treatment of abnormal chest wall, minimally invasive chest surgery, and laser applications in surgery and medical science. He has authored more than 30 papers in the field of thoracic surgery and laser application in medicine.

**Huajiang Wei** is an associate professor in the MOE Key Laboratory of Laser Life Science at South China Normal University. His research interests include measure and control of optical properties of tissues and blood, diagnostic spectroscopy, medical imaging, and the application of optics in medicine. He has authored more than 60 papers in the field of tissue optics, optical diagnosis, and therapy principle and techniques.

**Zhouyi Guo** is a professor in the MOE Key Laboratory of Laser Life Science at South China Normal University. His research interests include optical imaging techniques for live cells or tissues and their applications in biomedicine. He has authored more than 90 papers in the field of biomedical photonics.

**Hongqin Yang** received his PhD degree in optical engineering from Zhejiang University in 2007. He works at Fujian Normal University and was an associate professor of optical engineering from 2008. His research interests include optical imaging techniques for live cells or organisms and their applications. He has published over 30 peer-reviewed articles and owns 5 patents.

**Yonghong He** is the director of Laboratory of Optical Imaging and Sensing, Graduate School at Shenzhen, Tsinghua University. His research interests include surface plasmon resonance biosensing and optical coherence tomography. He has authored more than 30 peer-reviewed papers. He has been awarded Shenzhen Natural Science Funds for Distinguished Young Scientists, 2010, and Award of Science and Technology, Guangdong province, China, 2005.

**Shusen Xie** is the head of the Laser and Photoelectronic Technology Institute at Fujian Normal University, vice chairman of the Chinese Optical Society. He completed a postdoctoral fellowship in laser biomedical engineering from the University of California. He is the guest professor of the College of Science in Singapore Nanyang Technological University. He has authored more than 200 peer-reviewed papers and has gained 15 scientific and technological fruit awards at or above the provincial level.

**Ying Liu** is a graduate student in the MOE Key Laboratory of Laser Life Science and the Institute of Laser Life Science, College of Biophotonics at South China Normal University, China. Her research interests include noninvasive blood glucose monitoring and histological diagnosis with optical properties using optical coherence tomography.

**Qingan Meng** is an engineer at Southwest Institute of Technical Physics, Sichuan, China. He is mainly engaged in measurement and application of the physics characteristics of nanometer materials.